THE JOURNAL OF PHYSICAL CHEMISTRY C

Article

pubs.acs.org/JPCC

Dynamics of Interfacial Electron Transfer from Betanin to Nanocrystalline TiO_2: The Pursuit of Two-Electron Injection

Fritz J. Knorr,[†] Jeanne L. McHale,*[,†] Aurora E. Clark,[†] Arianna Marchioro,[‡] and Jacques-E. Moser[‡]

[†]Department of Chemistry, Washington State University, Box 644630, Pullman, Washington 99164-4630 United States

[‡]Photochemical Dynamics Group, Institute of Chemical Sciences and Engineering, École Polytechnique Fédérale de Lausanne, CH-1015 Lausanne, Switzerland

Supporting Information

ABSTRACT: We report spectroelectrochemical and transient absorption spectroscopic studies of electron injection from the plant pigment betanin (Bt) to nanocrystalline TiO_2. Spectroelectrochemical experiments and density functional theory (DFT) calculations are used to interpret transient absorption data in terms of excited state absorption of Bt and ground state absorption of oxidation intermediates and products. Comparison of the amplitudes of transient signals of Bt on TiO_2 and on ZrO_2, for which no electron injection takes place, reveals the signature of two-electron injection from electronically excited Bt to TiO_2. Transient signals observed for Bt on TiO_2 (in contrast to ZrO_2) on the nanosecond time scale reveal the spectral signatures of photo-oxidation products of Bt absorbing in the red and the blue. These are assigned to a one-electron oxidation product formed by recombination of injected electrons with the two-electron oxidation product. We conclude that whereas electron injection is a simultaneous two-electron process, recombination is a one-electron process. The formation of a semiquinone radical through recombination limits the efficiency and long-term stability of the Bt-based dye-sensitized solar cell. Strategies are suggested for enhancing photocurrents of dye-sensitized solar cells by harnessing the two-electron oxidation of organic dye sensitizers.

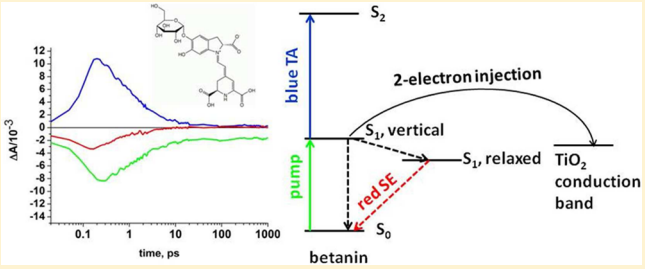

INTRODUCTION

Although dye-sensitized solar cells[1,2] offer a promising alternative to the present generation of photovoltaic devices, their economical and environmental advantages are offset by reliance on synthetic organic[3] and metal-organic[4] sensitizers. In the latter category, Ru-based dyes offer stability advantages owing to the reversible redox chemistry of the $Ru^{2+/3+}$ center, but ruthenium is a rare and expensive metal. Consequently, there is much interest in replacing synthetic sensitizers with organic pigments derived from plants.[5] One-electron oxidation of organic compounds, on the other hand, results in the formation of free radicals, which can pose stability problems for the solar cell. In the present work, we explore the question of harnessing the proton-coupled two-electron oxidation of a plant-based dye sensitizer, betanin, which we[6−8] and others[9−11] have previously used in TiO_2-based dye-sensitized solar cells (DSSCs).

Betanin (Bt, **I** of Figure 1) belongs to the betalain family of plant pigments, which comprises the purple betacyanins and yellow betaxanthins. These pigments are found in plants of the order Caryophyllales and play photoprotective and antioxidant roles.[12] Betacyanins are Schiff base adducts of betalamic acid (**II** of Figure 1) with cyclo-DOPA derivatives such as cyclo-DOPA 5-*O*-glucoside in the case of Bt. The yellow betaxanthins, of which indicaxanthin (In, **III** of Figure 1) is an example, are Schiff base linkages of betalamic acid with amino acids or amines. Owing to their nutritional advantages as antioxidants and their applications as food colorants, the redox properties of betalain compounds have been of great interest to the food science community.[13−17] The radical scavenging ability of betacyanins is correlated to the phenolic groups, and recently the molecular details of their oxidation have begun to emerge.[18−20] In ref 15, three oxidations of Bt were detected at 0.62, 0.84, and 1.2 V NHE, whereas two oxidations of In were observed at 0.84 and 1.2 V. This indicates that the first oxidation of Bt involves the aromatic ring or the sugar group.[21] An early study by Martínez-Parra and Muñoz[13] used horseradish peroxidase to oxidize betanin and found an oxidation intermediate with an absorption maximum similar to that of betanin (~530 nm) and a yellow final oxidation product (λ_{max} = 446 nm), which they assigned to betalamic acid. However, more recent studies assign λ_{max} of betalamic acid to be about 420 nm.[22] Wybraniec et al. have reported enzymatic and electrochemical oxidation of betanin and its aglycone betanidin (Bd).[18] The electrochemical oxidation of Bd was found to proceed by a two-electron, one-proton process in the pH range of 3−5 and by a two-electron, two-proton process in the pH range of 6−8. Enzymatic oxidation of Bt[19] was observed to lead

Received: June 19, 2015
Revised: July 28, 2015
Published: July 30, 2015

DOI: 10.1021/acs.jpcc.5b05896
J. Phys. Chem. C 2015, 119, 19030−19041

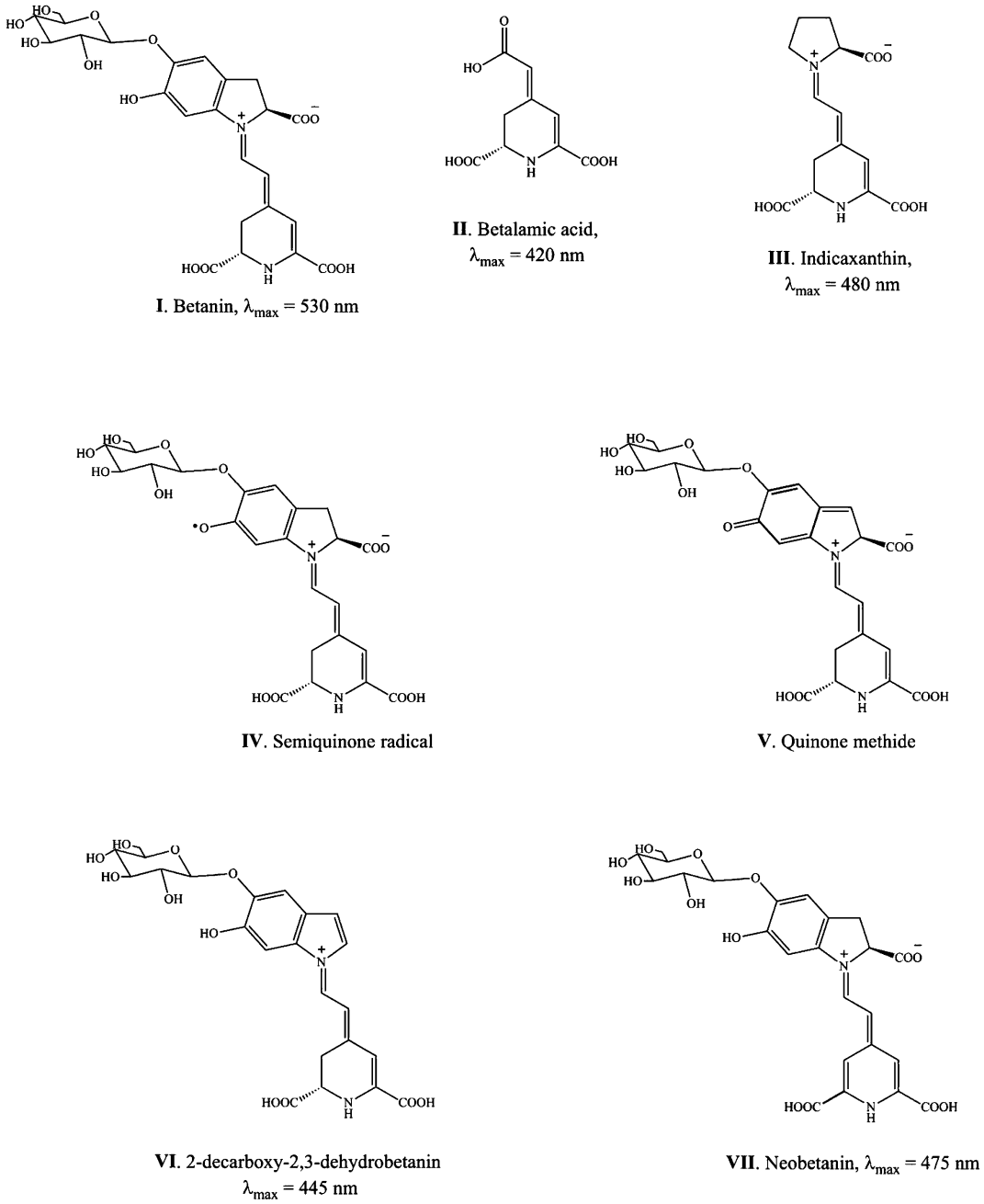

Figure 1. Betalain molecules.

to the two-electron oxidation product 2-decarboxy-2,3-dehydrobetanin (dhBt, **VI** of Figure 1), presumably through rearrangement of the quinone methide intermediate (QM, **V** of Figure 1). dhBt, for which λ_{max} = 445 nm, was observed to undergo further oxidation and decarboxylation. Chemical oxidation of Bt by ABTS radical, 2,2′-azinobis(3-ethylbenzthiazoline-6-sulfonic acid), also leads to formation of dhBt[20] and was presumed to take place via the one-electron oxidation product, semiquinone radical (SQ, **IV** of Figure 1), as an intermediate. Another possible two-electron, two-proton oxidation product is yellow neobetanin (**VII** of Figure 1), which has been observed to form in thermally treated extracts of red beet root.[23] Melanogenesis, or polymerization to form brown pigments similar to those found in the biological pigment eumelanin,[24] is another possible oxidative degradation product of betanin and other betacyanins. These polymers form on cross-linking of monomers of dihydroxyindole and derivatives and show spectral shifts associated with noncovalent interactions.[25,26] The absorption spectrum of these polymeric products is a monotonically decreasing function of wavelength, and increased absorption at red wavelengths has been suggested to result from aggregation via π-stacking.

In the present work, we consider electron injection from electronically excited Bt to nanocrystalline TiO_2. Scheme 1 summarizes the possible formation of the two-electron oxidation product, dhBt, via a sequence of two one-electron, one-proton oxidations. Although the ultimate two-electron oxidation product is stable and has an absorption wavelength of 445 nm, neither the one-electron oxidation product, a semiquinone radical, nor the two-electron quinone methide intermediate has been isolated, and their absorption wavelengths are unknown. We thus use density functional theory

DOI: 10.1021/acs.jpcc.5b05896
J. Phys. Chem. C 2015, 119, 19030−19041

Scheme 1. Possible Pathway from Bt to dhBt

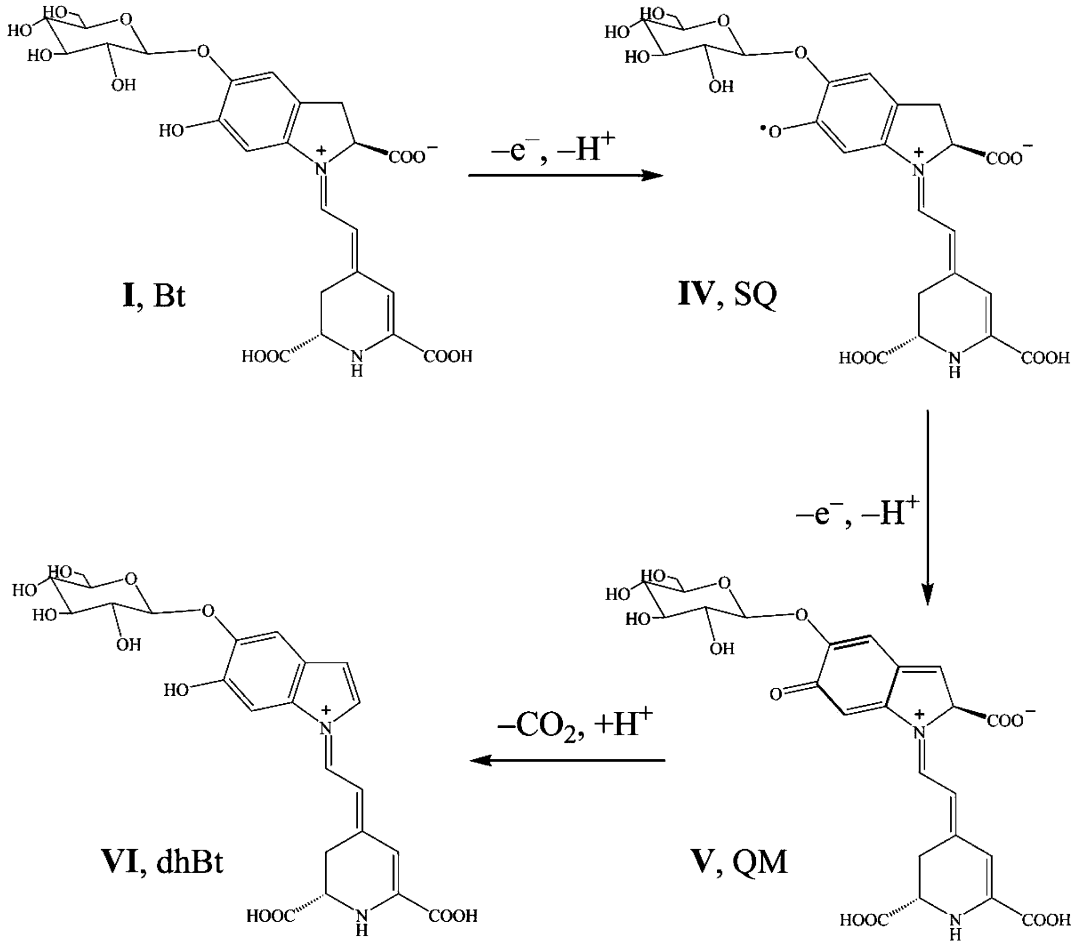

(DFT) calculations to estimate the absorption wavelengths for comparison to what is observed in transient absorption spectroscopy.

Interest in the potential for two-electron oxidation of Bt stems from our previous reports of nearly 100% maximum incident photon-to-current conversion efficiency (IPCE).[7] Because those IPCE data were not corrected for inevitable absorption and reflection losses, and because our reported open-circuit voltages are suggestive of recombination losses, we have postulated that Bt is capable of carrier multiplication via injection of two electrons per photon. We have previously shown[27] that the redox potential of aqueous Bt, observed at 0.65 V versus Ag/AgCl (0.86 V NHE) at pH 1.8, shifts negatively by 34 mV/pH as the pH is increased. This is consistent with a two-electron, one-proton oxidation, as proposed in Scheme 1. Also reported in ref 27 were our spectroelectrochemical data for Bt adsorbed on a nanocrystalline TiO_2 electrode showing the formation of an oxidation product with an absorption maximum at 445 nm, assigned to the two-electron oxidation product dhBt. We also presented our transient absorption data for Bt on nanocrystalline TiO_2 and ZrO_2 on femtosecond and nanosecond time scales. When Bt is adsorbed on ZrO_2, no photo-oxidation takes place, and the resulting purple films are stable on exposure to laser radiation and with long-term storage. The absence of any transient features in the nanosecond absorption spectrum of Bt on ZrO_2 indicates that the transients seen for Bt/TiO_2 on this time scale, that is, positive absorption bands in the red and blue, are oxidation products rather than excited state absorption. Because only the 445 nm absorption band is seen in steady state absorption spectra of Bt/TiO_2 after laser exposure, we consider here whether the red absorption band observed on a nanosecond time scale, at ~650−750 nm, could be a one-electron oxidation product or other intermediate in the formation of dhBt.

In this work, we consider two possible mechanisms for two-electron injection: a single-step process consistent with a merger of the first and second one-electron oxidation potentials and a current-doubling mechanism resulting from the second redox potential of Bt being more negative than the redox potential of the TiO_2 conduction band. We consider the thermodynamics of electron injection and dye regeneration and propose ways to address the stability issues associated with photo-oxidation of betanin and related molecules on TiO_2.

■ EXPERIMENTAL SECTION

Purification. Betanin was extracted and purified from red beet root as described in ref 7 and recrystallized as described in ref 27. HPLC confirmed the presence of betanin and the C-15 epimer isobetanin in solutions used to sensitize TiO_2 films. For transient absorption measurements, ~2 μm thick films of TiO_2 (anatase) or ZrO_2 nanoparticles (particle size ~ 20 nm) were soaked overnight in ~1 μM aqueous Bt solution at a pH of approximately 3. The resulting sensitized films gave absorption maxima near 500−520 nm with optical density in the range 0.5−1. Absorption spectra were monitored before and after

DOI: 10.1021/acs.jpcc.5b05896
J. Phys. Chem. C 2015, 119, 19030−19041

laser exposure to assess degradation. Transient absorption spectra were recorded for films in contact with methoxypropionitrile (MPN) or 0.5 M LiI in MPN as indicated in the text.

Spectroelectrochemistry. The samples for the spectroelectrochemical studies used 4 μm thick mesoporous anatase films on TEC 15 conductive glass. These were stained with an aqueous 3 mM betanin solution, pH 3.2. The darkness of the film was varied using soaking times from 15 s to 20 min. The stained film was immersed in a cuvettte filled with 0.2 M $NaClO_4$ in acetonitrile. The absorbance was measured on a Shimadzu 2501 spectrophotometer versus air. Potentials were applied with BAS 100A potentiostat, with a Ag/AgCl reference and Pt wire counter electrode. Each difference spectrum shown in Figure 2 is the difference between the absorbance at 0 V and at the applied potential after 1.0 mC of charge was passed.

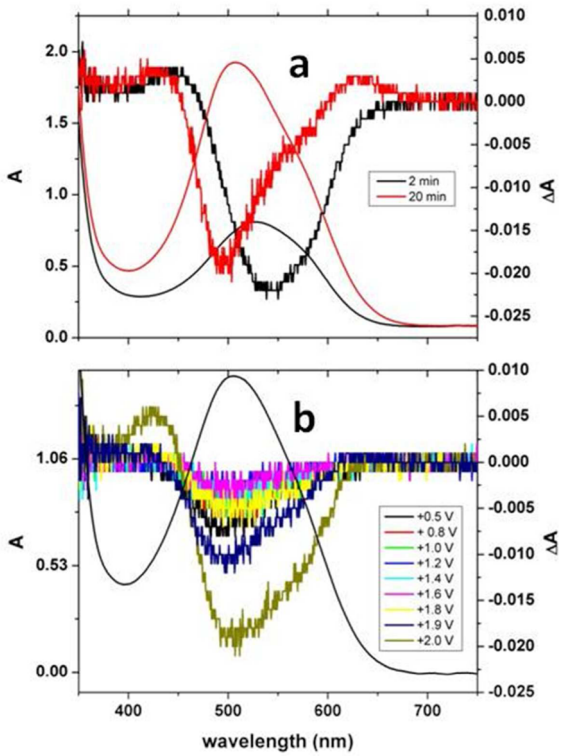

Figure 2. (a) Absorption spectra of a Bt-sensitized TiO_2 film at open circuit after soaking times of 2 min (black) and 20 min (red) (left axis, smooth curves) and corresponding difference SEC spectra at 2.0 V (right axis, noisy curves). (b) Absorption spectrum at open circuit of a film sensitized for 15 min and difference spectra of the same film as a function of applied voltage.

Transient Absorption Spectroscopy. Femtosecond and nanosecond transient absorption spectra were recorded as described in ref 27. Briefly, femtosecond pump−probe spectra were recorded at an excitation wavelength of 580 nm generated by a non-collinear optical parametric amplifier from the output of a Ti:sapphire laser at 778 nm, resulting in sub-50 fs pulses after compression. The white light probe, 400−750 nm, was generated by passing a portion of the 778 nm Ti:sapphire output through a CaF_2 crystal. Nanosecond transient absorption spectra were excited with the 532 nm output of a frequency-doubled Q-switched Nd:YAG laser. The probe wavelength was selected by a monochromator from a cw Xe arc lamp source, and the transmitted light was detected by a fast photomultiplier tube.

Computational Methods. The gas phase structures of molecules **I**, **IV**, **V**, and **VI** (Figure 1) were optimized using the Gaussian 09[28] electronic structure software program and using the B3LYP[29,30] combination of density functionals with the cc-pVDZ[31,32] basis set describing the atomic orbitals of all atoms. After optimization of the ground state for each species, single-point time-dependent DFT (TD-DFT) calculations were then employed to calculate the spectrum of allowed optical excitations, up to the 20th singlet excited state. Due to the range of electronic structures in molecules **I**, **IV**, **V**, and **VI** (zwitterions, cations, and radicals), the ability of a single density functional to accurately predict the range of potential excitation types (e.g., charge transfer) is limited, and benchmarking studies must be performed to determine which method is most appropriate for the entire molecular series.

Three density functionals were utilized for these TD-DFT benchmark studies: B3LYP, cam-B3LYP,[33] and LC-ωPBE.[34−37] B3LYP is a global hybrid combination of exchange-correlation functionals that includes 20% exact HF exchange and for benchmark sets of compounds (e.g., the molecular ensemble of Thiel and collaborators, proposed in 2008[38−40]) typically results in TD-DFT errors of vertical singlet excitation energies on the order of 0.25−0.4 eV[41,42] in the gas phase. Yet B3LYP suffers from a well-known inability to appropriately treat long-range behavior, as is typical in charge-transfer transitions, and as such underestimates the vertical CT excitation energies.[43] Density functionals that have various amounts of HF exchange at different interatomic distances are labeled as range-separated hybrid (RSH) or long-range corrected density functionals (LC-DFT) and are generally accepted as viable options for describing CT phenomenona.[32,34,44,45] This class of density functionals includes cam-B3LYP and LC-ωPBE, which have been demonstrated to yield reasonable errors of 0.2−0.4 eV for CT transition energies, although they exhibit varying performance for standard $n-\pi^*$ and $\pi-\pi^*$ excitations.[39,40,46]

The solution phase environment must also be accounted for, and in this work a QM/continuum approach is employed where the TD-DFT excitation occurs within the solute that is embedded in a dielectric continuum that approximates the effect of the bulk solvent. The integral-equation-formalism-protocol (IEF) polarizable continuum model (denoted IEF-PCM) using the default UFF cavity, the IEF model using the radii, and nonelectrostatic terms of Truhlar and co-workers' SMD solvation model in Gaussian 09,[47] and the conductor-like polarizable continuum model (CPCM) using the default UFF cavity were each used.

To benchmark the computational protocol for the two molecules **I** (Bt) and **VI** (dhBt) that have known UV−vis spectra, a multistage approach was taken. First, the gas phase geometries of **I** and **VI** were optimized and the three PCM approaches were used in conjunction with the three density functionals to calculate the transition energies for the first 20 singlet states (at the gas phase geometry), which were then compared to the experimentally obtained λ_{max} values in water. The best functional and PCM that could reproduce the trends in the absorption maxima were then elucidated (Table S1 in the Supporting Information). As demonstrated in Table S1, the cam-B3LYP combination of functions either in the gas phase or with the CPCM or IEF-PCM solution models can correctly approximate the 85 nm shift of **I** (Bt) going to **VI** (dhBt). Interestingly, B3LYP either in the gas phase or with the

DOI: 10.1021/acs.jpcc.5b05896
J. Phys. Chem. C 2015, 119, 19030−19041

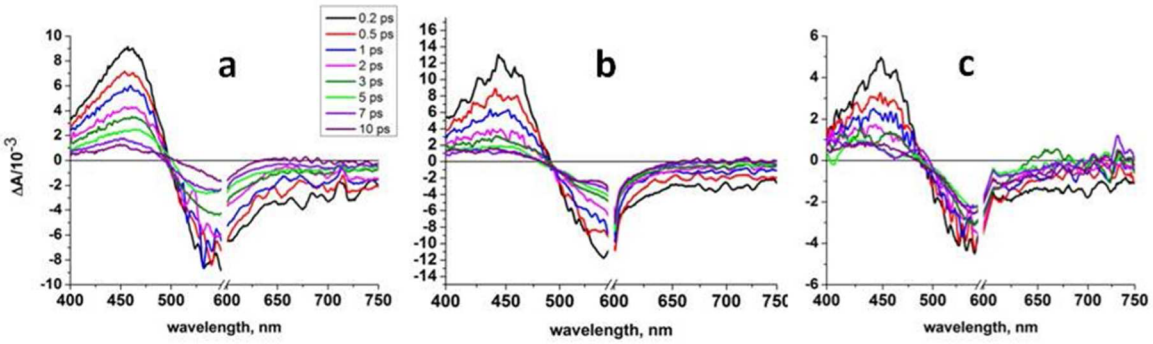

Figure 3. Femtosecond transient absorption spectra recorded with a pump wavelength of 580 nm for (a) Bt on ZrO_2 in contact with MPN, (b) Bt on TiO_2 in contact with MPN, and (c) Bt on TiO_2 in contact with MPN and LiI.

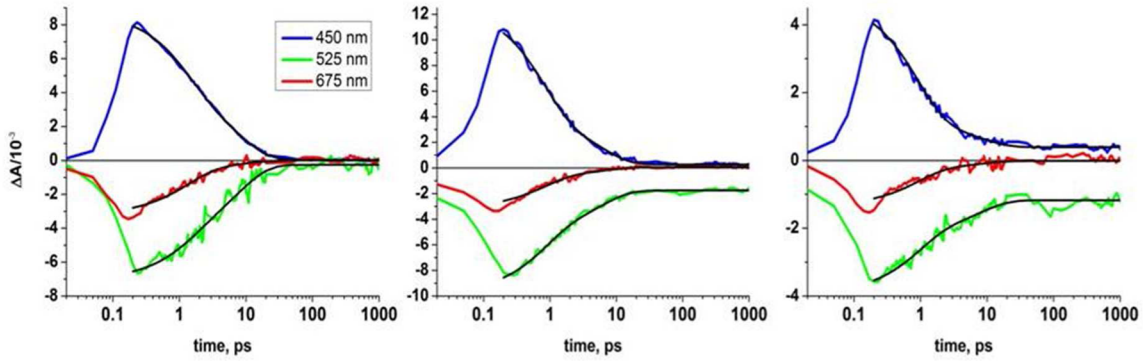

Figure 4. Femtosecond transients for selected probe wavelengths, recorded with a pump wavelength of 580 nm for (a, left) Bt on ZrO_2 in contact with MPN, (b, middle) Bt on TiO_2 in contact with MPN, and (c, right) Bt on TiO_2 in contact with MPN and LiI. Black lines are the results of global fits to a biexponential decay plus a nondecaying background at the respective wavelength.

Table 1. Amplitudes (ΔA in Milliabsorbance Units) and Backgrounds y_0 at 450, 525, and 675 nm[a]

	decay times, ps		450 nm			525 nm			675 nm		
	τ_1	τ_2	A_1	A_2	y_0	A_1	A_2	y_0	A_1	A_2	y_0
Bt/ZrO_2	1.3	8.1	4.03	4.62	0.030	−4.31	−2.44	−0.25	−0.61	−2.56	0.0034
Bt/TiO_2	0.79	5.9	8.70	3.63	0.273	−4.70	−3.26	−1.76	−2.44	−0.75	0.0503
$Bt/TiO_2/LiI$	0.90	7.7	3.59	0.77	0.391	−1.71	−1.02	−1.18	−1.08	−0.26	−0.010

[a] A_1 and A_2 are the respective amplitudes of the fast (τ_1) and slow (τ_2) components of the decay.

continuum models can also predict the correct trend, although to a lesser extent than cam-B3LYP. The lc-ωPBE functional in the gas phase predicts the correct trend, but upon immersion in a continuum dielectric, the trend changes and the opposite behavior is observed. Given the electronic structure of the remaining molecules **IV** and **V** and the high likelihood of charge transfer character in their electronic transitions, the cam-B3LYP method was chosen to determine their vertical excitation energies, alongside the IEF polarizable continuum model to approximate the solution phase effects.

■ RESULTS

Spectroelectrochemistry. As previously shown,[27] a Bt-sensitized TiO_2 electrode held at 2 V versus Ag/AgCl develops a shoulder at 445 nm consistent with formation of the two-electron oxidation product **VI**. Figure 2 shows changes to the open circuit absorption spectrum and the spectroelectrochemical (SEC) difference absorption spectra of Bt on TiO_2 as a function of dye loading. As shown in Figure 2a, a film sensitized for 2 min in aqueous Bt results in a spectrum at open circuit with a maximum at about 530 nm, similar to that for Bt in solution. The difference SEC spectrum of this film shows a dip at 540 nm and a weak positive ΔA at about 450 nm. A film soaked for 20 min, however, exhibits an absorption maximum of 507 nm at open circuit, and the SEC difference spectrum exhibits a negative ΔA at 500 nm and positive features in both the blue (~430 nm) and the red (~640 nm). We note that very low dye loadings (not shown) result in a more typical red-shifted absorption spectrum with maxima near 540 nm. The general blue shift in the spectrum of Bt with higher dye loading was also observed on nanocrystalline ZrO_2 as shown in Figure S1 of the Supporting Information. As seen in Figure 2b, there is an abrupt increase in the negative feature at ~530 nm, corresponding to the disappearance of Bt, and an increase in the positive ΔA feature with a peak at about 420−430 nm, in the range 1.8−2.0 V.

Femtosecond Transient Absorption Spectra. Figure 3 shows transient spectra at selected time delays from 0.2 to 10 ps for Bt on ZrO_2, on TiO_2, and on TiO_2 in the presence of LiI to regenerate the dye after oxidation. The films were wetted with neat MPN or a solution of 0.5 M LiI in MPN. In all cases there is a positive transient absorption with a maximum near

DOI: 10.1021/acs.jpcc.5b05896
J. Phys. Chem. C 2015, 119, 19030−19041

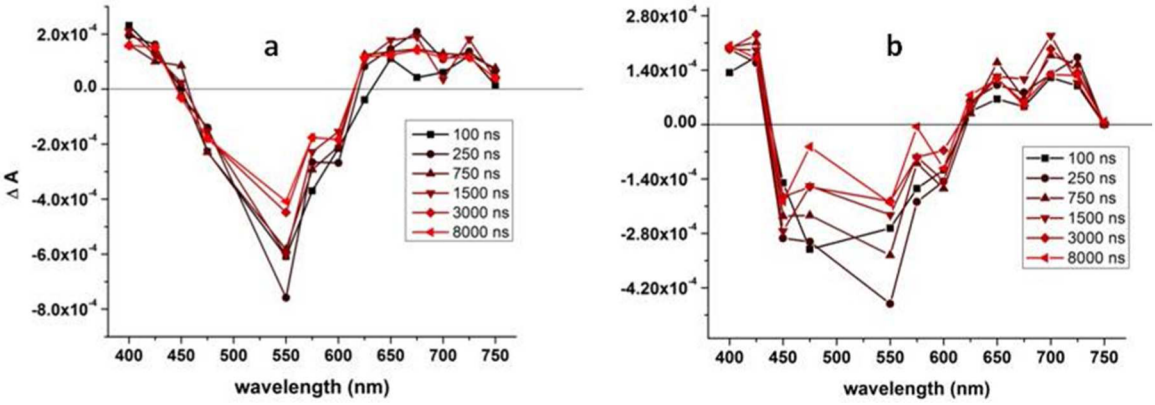

Figure 5. Nanosecond transient spectra of Bt on TiO_2 in contact with MPN (a, left) and with PMII electrolyte (b, right).

450 nm, a bleach in the green corresponding to ground state depletion, a negative transient at wavelengths in the ~650−750 nm range, and an apparent isosbestic point at about 500 nm.

Figure 4 shows the dynamics at selected wavelengths for the same data as shown in Figure 3. The increase in the positive ΔA at blue wavelengths appears to parallel the increase in the negative ΔA at longer wavelengths. It is thus reasonable to interpret the data in Figures 2 and 3 to reflect excited state absorption at blue wavelengths, the expected ground state bleach in the green, and apparent stimulated emission in the red. The latter is consistent with the wavelength range of the steady state fluorescence spectrum of Bt.[27] The results of global fits to a biexponential relaxation model plus a constant background (nondecaying on the ps time window of our experiment) were reported in ref 27 and are shown graphically in the Supporting Information (Figure S2).

Table 1 summarizes the results from a multiexponential global analysis of the transient absorption dynamics at selected wavelengths (450, 525, and 675 nm). Figure 4 compares the experimental data to the resulting fits (plotted from 0.2 to 1000 ps to capture the decay). The dynamics in all three samples are accounted for with a model of biexponential relaxation characterized by one shorter (~1 ps) and one longer (6−8 ps) decay time, plus a nondecaying residual component y_0. Table 1 gives the amplitudes of the fast (A_1) and slow (A_2) components of the transient absorption (TA) at 450 nm, the bleach at 525 nm, and the stimulated emission (SE) at 675 nm. The TA in the blue decays on both time scales, as does the green bleach. The red SE, on the other hand, decays mostly on the faster time scale in the case of Bt on TiO_2, but has a larger amplitude of slow decay for Bt on ZrO_2. Although the fast and slow relaxation times are not significantly different for the three samples, the amplitudes of the global fits (Figure S2 and Table 1) vary. First, there is a persistent green bleach and a small positive blue ΔA in the nondecaying trace for the two Bt/TiO_2 samples, compared to a flat residual ΔA for Bt/ZrO_2. This is consistent with partial irreversible oxidation of Bt on TiO_2 but not on ZrO_2, in agreement with the comparison of steady state absorption spectra of the films before and after laser exposure.[27] Second, the relative amplitudes of the fast and slow decay components differ greatly, especially when looking at the positive transient in the vicinity of 450 nm. For Bt on ZrO_2, the fast component of the blue TA has an amplitude similar to that of the slow component. For Bt on TiO_2 in the absence of electrolyte the fast decay of the blue transient has an amplitude ~2.4 times greater than that of the slow decay, and in the presence of LiI this ratio increases to ~4.7. We attribute the increase in the relative amplitude of the fast decay on TiO_2 to the additional fast relaxation resulting from electron injection. The amplitudes of the fast and slow decays of the green bleach also vary. On ZrO_2, the depth of the bleach at short time is comparable to the amplitude of the fast blue TA. For the two TiO_2 samples, the relative amplitude A_1 at 525 nm is reduced compared to A_1 at 450 nm. The dynamics of the red SE also differ for Bt on ZrO_2 compared to TiO_2, with a larger component of slow decay relative to fast on ZrO_2. On TiO_2, the SE decays more on the shorter time scale. This is consistent with the formation of product that absorbs in the red on the longer time scale for the two TiO_2 samples, offsetting the red SE. As shown below, the nanosecond spectra do show a red TA for Bt on TiO_2 but not on ZrO_2.

Interpretation of these data is clouded by the apparent coincidence of the wavelengths for the putative $S_1 \rightarrow S_2$ transition of Bt and the $S_0 \rightarrow S_1$ transition of the two-electron oxidation product dhBt at 445 nm. The latter is known from experiment, and the former implied by the femtosecond transient absorption of Bt on ZrO_2. However, if we make the reasonable assumption that the oscillator strength of the 445 nm transition of dhBt is smaller than that for the $S_1 \rightarrow S_2$ transition of Bt (vide infra), then we can interpret the above results as follows. For Bt on ZrO_2, we assume no formation of dhBt and assign the fast (~1 ps) decay component at 450 nm to relaxation of the vertically excited (Franck−Condon) electronic state to the equilibrium geometry of the S_1 excited state, whereas the slower decay component results from direct decay of the vertically excited state to the ground state. Support for this interpretation can be found in examining the transient spectra of Bt on ZrO_2 in Figure 3a, where perceptible shifts in the absorption maximum are observed, from about 455 nm at 0.2 ps to about 470 nm at 5 ps and then back to 450 nm from 5 to 10 ps. For Bt on TiO_2 as compared to on ZrO_2, the amplitude of the fast component is increased relative to the slow (6−8 ps) component, more so in the presence of LiI. We attribute this to the additional fast decay channel of electron injection from the vertically excited state to TiO_2. It is well-known that Li^+ lowers the conduction band energy of TiO_2,[48] resulting in a greater driving force for electron injection and a greater amplitude of fast decay of the S_1 excited state of Bt.

For the above interpretation to be viable, we must assume that the oscillator strength of the excited state absorption of Bt is greater than that of the ground state absorption of dhBt. The low oscillator strength of the latter, at least relative to that of

DOI: 10.1021/acs.jpcc.5b05896
J. Phys. Chem. C 2015, 119, 19030−19041

the $S_0 \rightarrow S_1$ transition of Bt, is supported by the spectroelectrochemical data of Figure 2, as well as the spectra shown for enzymatic oxidation of Bt in Figure S3 of the Supporting Information. We cannot rule out the possibility, as suggested by ref 13, that the initial oxidation of Bt leads to a species with an absorption maximum (530 nm) similar to that of Bt, but lower molar absorptivity. The formation of such a product (on TiO_2 but not on ZrO_2) could be responsible for the aforementioned difference in the depth of the bleach relative to the blue TA; the green TA of this oxidation product would partially offset the bleach from ground state depletion of Bt. However, the apparent isosbestic point at about 500 nm for Bt on both TiO_2 and ZrO_2 indicates that in both cases the excited state relaxation regenerates the ground state dye. The existence of an excited state absorption at 450 nm (22000 cm^{-1}), combined with the ground state absorption of Bt at 530 nm (19000 cm^{-1}), suggests a putative $S_0 \rightarrow S_2$ transition that, if allowed, would be observed at 240 nm (41000 cm^{-1}). This is in moderately good agreement with the observed doublet of UV transitions of Bt at 290 nm (34500 cm^{-1}) and 270 nm (37000 cm^{-1}), as seen in the black trace of Figure S3 of the Supporting Information. However, we are using solution phase data for these estimates, and the shift of the UV transition of Bt on adsorption on TiO_2 cannot be discerned owing to overlap with the strong bandgap transition of the semiconductor.

Nanosecond Transient Absorption Spectra. The nanosecond transient absorption spectrum of Bt on TiO_2 shows positive features at blue and red wavelengths and a negative transient absorption at green wavelengths. Figure 5 shows transient spectra at time delays from 100 to 8000 ns for Bt on TiO_2 in the presence of neat MPN and neat 1-propyl-3-methylimidazolium iodide (PMII), an ionic liquid that serves as a reductant. The latter is seen to lead to regeneration of Bt as revealed by the faster decay of the green bleach compared to the sample in MPN. Figure S4 shows the results of fitting the transients at 425, 600, and 670 nm to a single exponential decay. The decay times are respectively 2.0, 2.5, and 2.2 μs, essentially the same within error. The transients do not decay to zero on the time scale of the experiment. The persistence of the features at 425 and 600 nm wavelengths is consistent with the appearance of the steady state absorption spectrum of the sample after laser exposure (see ref 27), which shows a decrease in the ground state Bt absorption and an increase in absorption in the blue with a peak or shoulder at 450 nm. However, no red absorption bands in the range from 650 to 700 nm were seen in the spectra of films that had been subjected to transient absorption measurements. Thus, we turned to theoretical calculations to attempt to associate the red absorption band in the nanosecond spectra with a possible intermediate.

DFT Calculations. As mentioned above, the series of molecules **I** − **VI** span a large range of electronic structure, and consequently variable types of excitations will contribute to their absorption spectra. Given this complexity, it is a challenging task to find a DFT method/basis set and PCM that will treat all types of excitations on equal footing. Thus, the focus of this work is to utilize a computational approach that correctly reproduces the trends in the known absorption spectra instead of the absolute values of λ_{max}. As demonstrated in Table S1, the cam-B3LYP range-corrected hybrid density functional using IEF-PCM calculates a 23 nm (0.14 eV) shift in the absorption maximum when going from molecule **I** to **VI**, which compares well to the experimental 85 nm (0.45 eV) shift. The agreement between experiment and theory is within the error in the calculation. The underestimation in the shift value derives largely from the overestimation in the transition energy for **I** Bt, which has a predicted transition energy that is blue-shifted relative to experiment by 74 nm. Table 2 reports the calculated wavelengths and oscillator strengths of the electronic transitions of Bt (**I**), the semiquinone radical (**IV**), the quinone methide intermediate (**V**), and the two-electron oxidation product dhBt (**VI**). The agreement of the trends in absorption spectra (peak position and intensity) is reserved for the Discussion.

Table 2. Calculated Transition Wavelengths and Oscillator Strengths

	calculated electronic transitions	
	$S_0 \rightarrow S_1$	$S_0 \rightarrow S_2$
I Bt	456 nm	348 nm
	f = 1.1	f = 0.22
	calculated electronic transitions	
	$S_0 \rightarrow S_1$	$S_0 \rightarrow S_n$ (max f)
IV SQ	757 nm	354 nm
	f = 0.003	f = 0.65
V QM	464 nm	464 nm
	f = 0.9	f = 0.9
VI dhBt	485 nm	431 nm
	f = 0.40	f = 0.93

For **IV**, **V**, and **VI** we report the wavelength and oscillator strength of the lowest lying transition and those of the strongest optical transition. With the exception of Bt, only electronic transitions originating in the ground electronic state are considered relevant. For **IV**, **V**, and **VI**, both the lowest lying and the strongest electronic transitions are reported. For **VI**, two low-lying transitions carry similar oscillator strength, leading to a predicted absorption maximum intermediate between the two as obtained by a simulation of the absorption spectrum. For Bt (**I**) at the cam-B3LYP level with the IEF-PCM water model, the ground state absorption is predicted at 456 nm compared to the experimental wavelength of 530 nm. The calculated oscillator strength of 1.1 is in good agreement with experiment (f = 1) based on the integrated absorption spectrum and a maximum molar absorptivity of 65000 M^{-1} cm^{-1}.[49] The $S_0 \rightarrow S_2$ transition of Bt is calculated at 348 nm with an oscillator strength of 0.23. The calculation cannot directly predict the oscillator strength or wavelength of the excited state absorption, but on the basis of the wavelengths of the $S_0 \rightarrow S_1$ and $S_0 \rightarrow S_2$ transitions from DFT, the $S_1 \rightarrow S_2$ transition of Bt would occur at only about 7000 cm^{-1}, in poor agreement with the observed excited state absorption at 450 nm or 22200 cm^{-1}. As previously mentioned, however, the wavelength of the putative $S_1 \rightarrow S_2$ transition observed in the femtosecond pump−probe experiment is in fair agreement with the value expected from the difference in the energies of the visible and UV transitions of Bt in aqueous solution. DFT results suggest that the UV bands at 270 and 290 nm in the ground state absorption of Bt result from transitions to states above S_2. Indeed, there are three predicted UV transitions of Bt in good agreement with experiment: the $S_0 \rightarrow S_5$ transition at 304 nm (f = 0.003), $S_0 \rightarrow S_6$ at 274 nm (f = 0.08), and $S_0 \rightarrow S_7$ at 259 nm (f = 0.008).

One the other hand, the calculated absorption maximum of dhBt (**VI**) at 455 nm is in good agreement with the

DOI: 10.1021/acs.jpcc.5b05896
J. Phys. Chem. C 2015, 119, 19030−19041

experimental value of 445 nm. In this case, the lowest lying transition is predicted at 485 nm, but a higher lying transition at 431 nm carries more oscillator strength, resulting in a predicted absorption maximum intermediate between the two but with a decreased intensity relative to that of Bt. The better agreement between theory and experiment for dhBt as compared to Bt, using cam-B3LYP, indicates more charge-transfer character for the former.

In the case of the semiquinone (**IV**) and quinone methide (**V**) intermediates, the absence of absorption data prevents comparison of DFT results with experiment. We report the results from DFT using the same basis set and PCM model as were used for **I** and **VI**. The $S_0 \rightarrow S_1$ transition of the SQ radical is predicted to occur at 757 nm, but with very low oscillator strength. The strongest transition is found at 354 nm. There are as many as four states between S_1 and the state that carries the most oscillator strength. QM (**V**), the proposed two-electron oxidation intermediate of Bt, has a predicted ground state absorption at 464 nm, with an oscillator strength of 0.9. The lowest lying transition has the largest oscillator strength in this case.

■ DISCUSSION

The spectroelectrochemical and transient absorption measurements presented here show evidence for the formation of the two-electron oxidation product of Bt, dhBt. Bt-sensitized TiO_2 films after laser exposure reveal the characteristic absorption band of dhBt at 445 nm.[27] The presence of a weak band at this wavelength in the absorption spectrum of Bt-sensitized TiO_2 biased at positive potential, in comparison to the large bleach of the Bt absorption at ∼530 nm, reflects the lower oscillator strength of the dhBt transition (as confirmed by the TD-DFT results) and/or formation of other products with weak absorption at visible wavelengths. The coincidence of the dhBt absorption with the excited state absorption of Bt complicates the interpretation of the femtosecond dynamics, but comparison of the data for Bt-TiO_2 and Bt-ZrO_2 reveals an additional fast quenching of Bt* on TiO_2 that is reasonably attributed to electron injection.

The question arises as to whether the two-electron oxidation of Bt on TiO_2 occurs simultaneously or sequentially. Let E_1^0 and E_2^0 be the standard redox potentials for the first and second redox steps, respectively:

$$\begin{aligned} &Bt^{\bullet+} + e^- \rightarrow Bt \qquad E_1^0 \\ &Bt^{2+} + e^- \rightarrow Bt^{\bullet+} \quad E_2^0 \end{aligned} \tag{1}$$

The participation of protons in the above steps is neglected for simplicity, as is the actual net charge of each molecule. In the normal situation, $E_2^0 > E_1^0$ and excited state Bt would be expected to inject a single electron forming the one-electron oxidation product $Bt^{\bullet+}$, presumably the semiquinone radical **IV**. Although such an intermediate would be unstable and thus not visible in steady state absorption measurements, we might have seen transient absorption from this species in the femtosecond measurements. The absorption wavelength of **IV** is not known experimentally. DFT calculations predict a strong near-UV transition for **IV** at 354 nm, which is outside the spectral window of our transient absorption measurements. DFT also predicts a weak absorption band of **IV** in the red, at about 757 nm. Perusal of the literature on transient absorption spectra of various semiquinone radicals reveals many that have both near-UV and red absorption bands,[50,51] validating the DFT results. Relevant to our system is the pulse radiolysis study of 5,6-dihydroxyindole-2-carboxylic acid,[52] which found a strong UV band of the initially formed semiquinone radical (the one-electron oxidation product), which decayed on a millisecond time scale to give a quinonoid species absorbing at 500−700 nm. We do see a positive transient at red wavelengths on longer time scales in the nanosecond data, for Bt on TiO_2, and comparison of the fast and slow components of the red SE in the femtosecond experiments also suggests formation of a red-absorbing species on the longer time scale in the TiO_2 samples. We conclude that a red-absorbing one-electron oxidation product, possibly SQ, forms on the longer time scale, whereas electron injection is seen on the shorter time scale. Thus, we propose that the semiquinone radical or other one-electron oxidation product forms by recombination of injected electrons with the two-electron oxidation product dhBt. Although we cannot completely rule out the possibility of single-electron injection from Bt* because the appearance of a femtosecond transient absorption from $Bt^{\bullet+}$ would be difficult to observe in the spectral window examined, our results are more consistent with a single-step, two-electron injection as discussed next.

In the case when the two-electron oxidation product is particularly stable, the redox potentials E_1^0 and E_2^0 may be similar or even inverted, leading to simultaneous two-electron transfer.[53,54] In this case the one-electron oxidation product should be thermodynamically unstable to disproportionation: $2Bt^{\bullet+} \rightarrow Bt^{2+} + Bt$. Disproportionation of the initially formed one-electron oxidation product in our SEC experiments, and when Bt is oxidized enzymatically,[13,14] would explain the apparent inability to completely convert Bt to dhBt. However, the steady state absorption spectra of Bt/TiO_2 following laser exposure show more complete conversion to the blue-absorbing product. On the basis of work by Wybraniec et al.,[18−20] two-electron injection from Bt* should result in the putative two-electron oxidation intermediate QM (**V**), the quinone methide, which then undergoes decarboxylation to form dhBt (**VI**). QM is predicted by DFT to have a maximum absorption at 464 nm with an oscillator strength of 0.9. This is quite close to the calculated λ_{max} of Bt at 456 nm, with an oscillator strength of 1.1. To the extent that errors in the DFT calculations are similar for Bt and QM, the results suggest that the transient absorption of the QM intermediate would be difficult to see, being overlapped by the ground state bleach of Bt at a similar wavelength (∼530 nm). Theory does, however, support the conclusions of refs 13 and14, which reported an oxidation intermediate of Bt with a similar absorption wavelength but reduced molar absorptivity. Quinone methides have been identified as intermediates in eumelanin biosynthesis, and a stable quinone methide has been prepared from the methyl ester of dopachrome, for which both deprotonation and decarboxylation are blocked.[55] Given that the maximum absorption of this species is at ∼420 nm, a somewhat longer predicted absorption wavelength of the more conjugated **V** is reasonable. Thus, the formation of QM in the femtosecond pump−probe experiments is difficult to observe directly owing to overlap with the bleach of Bt, but reveals itself in the comparison of the amplitude of the bleach relative to the blue TA.

Figure 6 illustrates four scenarios for electron injection from electronically excited Bt to the conduction band of TiO_2. We do not speculate on the formal redox potential for the ground state dye on TiO_2 except to assume that it is bracketed by the redox potential energies of the conduction band (CB) and

DOI: 10.1021/acs.jpcc.5b05896
J. Phys. Chem. C 2015, 119, 19030−19041

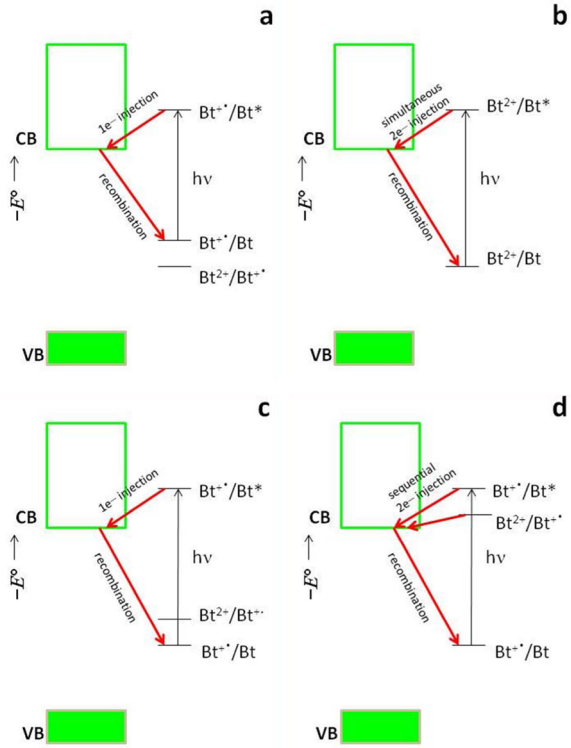

Figure 6. Possible mechanisms for the photo-oxidation of Bt on TiO_2: (a) one-electron injection with normal ordering of first and second redox potentials; (b) simultaneous two-electron oxidation and merging of first and second redox potentials; (c) inverted ordering of redox potentials and one-electron injection; (d) sequential two-electron injection via even greater inversion of first and second redox potentials.

valence band (VB). The SEC measurements of Bt on TiO_2 suggest that oxidation of Bt in its ground electronic state takes place in the vicinity of 1.9 V Ag/AgCl (2.1 V NHE). This is considerably more positive than the redox potential of Bt at a gold electrode in aqueous solution at pH 7, about 0.44 V Ag/AgCl,[27] perhaps as a result of the poor dark conductivity of the TiO_2 electrode. There is ample evidence that electron injection from Bt* to the CB of TiO_2 is thermodynamically favorable, resulting in good external quantum yields and energy conversion efficiency.[7] Considering an absorption onset of about 2 eV, our SEC measurements of Bt oxidation on TiO_2 would lead to an estimated excited state redox potential of about −0.1 V Ag/AgCl, which would result in insufficient driving force for excited state electron injection, given a redox potential energy for the conduction band of anatase TiO_2 of about −0.8 V Ag/AgCl. (We assume a CB redox potential in acetonitrile that is similar to that of water at pH 7 (see, for example, ref 56.)) Thus, it is apparent that there is an overpotential for the ground state oxidation of Bt on TiO_2, making it difficult to place the redox potentials relevant to excited state electron injection on an absolute scale.

The four mechanisms considered in Figure 6 are the following. In the normal ordering of redox potentials (Figure 6a), injection and recombination would take place as for a conventional one-electron dye sensitizer. The formation of the two-electron oxidation product Bt^{2+} would require absorption of a second photon by $Bt^{\bullet+}$, leading to electron injection from its excited electronic state. This mechanism could not lead to carrier multiplication. In the case when the first and second redox potentials merge, depicted in Figure 6b, both injection and recombination would be two-electron steps. Such a mechanism is plausible considering the observation of single-step electrochemical and enzymatic two-electron oxidation of ground state Bt in solution. Figure 6c considers inverted redox potentials, which would also lead to one-electron injection and recombination. However, now the one-electron product should undergo disproportionation, resulting in the formation of Bt^{2+} and Bt if recombination and regeneration are not sufficiently fast. This mechanism could not explain the high quantum efficiencies for electron injection that we have observed for some solar cells. The current-doubling mechanism (Figure 6d) could explain how two electrons result from one photon in the case when inversion of the redox potentials is so large that the redox potential of $Bt^{2+}/Bt^{\bullet+}$ is more negative than that of the TiO_2 CB. In this scenario, photon absorption by Bt leads to single-electron injection, followed by spontaneous injection of a second electron by $Bt^{\bullet+}$. This mechanism, similar to that for photocurrent doubling of UV-illuminated TiO_2 electrodes in the presence of alcohols,[57] would lead to carrier multiplication. However, it would pose problems for regeneration, because the redox potential of the $Bt^{2+}/Bt^{\bullet+}$ couple would be more negative than that of the redox mediator. Thus, this current-doubling mechanism cannot be reconciled with our reported stability measurements on Bt-sensitized DSSCs.[7]

The SEC data for Bt on TiO_2 at low dye loadings show the formation of a blue-absorbing species, with λ_{max} near 450 nm, at positive potentials. This is in accord with the two-electron oxidation product dhBt. However, the DFT calculations presented here also predict that the two-electron intermediate QM should also absorb in the blue. The persistence of the 450 nm absorption band following both SEC and transient absorption experiments argues for assigning it to the stable two-electron product dhBt and agrees with the observations of refs 18−20, which found λ_{max} = 445 nm for dhBt. At higher dye loadings, however, the SEC difference spectra show oxidization-associated absorption bands at 430 and 640 nm. The blue shift in the first feature relative to what is seen for lower dye loadings may signal the formation of betalamic acid as a result of dye degradation. However, the red absorption band, which goes hand-in-hand with the blue one for the darker film, is difficult to explain. We do not think this SEC feature correlates with the red absorption band seen in the nanosecond transient absorption, which, unlike its blue counterpart, is not present in the steady state spectrum of the film taken after laser exposure. The red absorption band seen in the SEC spectrum, on the other hand, is persistent and represents a stable product, the assignment of which eludes us at this point.

We attribute the spectral shifts to the blue in the SEC data for Bt on TiO_2 at higher dye loading to dye aggregation, to be discussed in a future publication. Transient absorption measurements on Bt-sensitized TiO_2 were made at relatively lower dye loading to get sufficient transmission of pump and probe beams, so these measurements would be less likely to be influenced by dye aggregation. Red-shifted spectra of dyes on TiO_2 relative to solution are common and result from electronic coupling of the dye and TiO_2.[58] Because a spectral blue shift of Bt on TiO_2 could also result from partial oxidation of Bt under room lights, we examined the spectra of Bt on ZrO_2. The observation of a similar blue shift for Bt on ZrO_2 at high dye loadings shows that the blue shift does not result from oxidation (Figure S1). Two-electron oxidation of cyclo-DOPA to form 5,6-dihydroxyindole carboxylic acid, which has a double bond in the five-membered ring, is a preliminary to the

DOI: 10.1021/acs.jpcc.5b05896
J. Phys. Chem. C 2015, 119, 19030−19041

formation of eumelanin[59] and is analogous to the formation of QM by oxidation of Bt. Certainly the covalent and noncovalent assembly of oxidized Bt by melanogenesis would be more facile for aggregated samples. This melanogenesis could be associated with the formation of a red-absorbing species in the SEC data for darker films, in agreement with calculations presented in ref 60, which attribute increased absorption in the red to noncovalent aggregation of melanin polymers. Whereas long-term storage of Bt-sensitized TiO_2 films does lead to a brown coloration, neither the SEC data nor the transient absorption data show evidence of quantitative formation of melanin, which is characterized by a spectrum in which absorption increases monotonically with decreasing wavelength. Certainly, the formation of melanin would not be conducive to long-term stability of the DSSC.

It is possible that this red TA in the nanosecond spectra derives from the absorption of conduction band electrons in TiO_2, which lead to absorption at wavelengths larger than 600 nm with a peak at about 750 nm.[61,62] This would explain its absence from the steady state absorption spectra obtained after laser exposure and would account for parallel decay of the blue and the red absorption bands on a $\sim 2\ \mu s$ time scale. However, the low molar absorptivity of conduction band electrons lends doubt to this hypothesis. We therefore assign the red and blue nanosecond transients to the dual absorption bands of SQ or a quinonoid decay product thereof, formed by recombination of injected electrons with QM. If a red absorbing one-electron oxidation product had formed via the current-doubling mechanism of Figure 6, decay of this transient by disproportionation would have led to a parallel rise in the blue-absorbing two-electron oxidation product, in contrast to the results of Figure 6.

Although laser excitation required for transient absorption measurements was found to result in irreversible degradation of Bt on TiO_2 (but not on ZrO_2), we have kept Bt-based DSSCs running for months at a time in our laboratory, albeit with gradual reduction in efficiency, which suggests that the dye is partially regenerated using an electrolyte containing the typical I_3^-/I^- redox couple. In the femtosecond pump−probe experiments, the sample was rotated to minimize degradation due to laser excitation. A sequential two-electron injection scheme such as that presented in Figure 6d would preclude regeneration by one-electron reduction of $Bt^{\bullet+}$ by I^- or by $I_2^{\bullet-}$, for which the one-electron reduction potentials are not more negative than the conduction band potential.[62] Thus, the model for sequential injection of two electrons from Bt* is inconsistent with stability data for DSSCs.

We are left with the mechanism shown in Figure 6b, simultaneous injection of two electrons from Bt* to TiO_2. Disappointingly, we cannot confirm the formation of QM as the initial two-electron oxidation product owing to the likely similarity of the ground state absorption spectra of Bt and QM. Looking at the global fits to the femtosecond data in Figure S2, it is apparent that the depth of the green bleach at short times relative to the positive absorption in the blue is larger for Bt on ZrO_2 compared to Bt on TiO_2. It is possible that this difference results from a positive absorption for QM in the green on the TiO_2 films, which partially offsets the bleach resulting from the ground state depletion of Bt. Although the forward electron transfer from Bt* to TiO_2 may be a single two-electron step, recombination of two injected electrons with Bt^{2+} seems less likely from a kinetic point of view as this would require two injected electrons in the vicinity of the oxidized molecule. Under normal conditions of a DSSC, only about 10 electrons are injected per nanoparticle, most of which are trapped.[63] Considering that there are hundreds of adsorbed dye molecules per nanoparticle, although few are oxidized, the availability of two injected electrons in the vicinity of an oxidized dye molecule is improbable. Thus, the recombination of injected electrons during the transient absorption measurements could be kinetically controlled, leading to the formation of $Bt^{\bullet+}$ through one-electron recombination with Bt^{2+}. We conclude that this recombination leads to the formation of $Bt^{\bullet+}$ on a nanosecond time scale, and that this species is responsible for the red and blue positive absorptions seen in the nanosecond data.

■ CONCLUSIONS

Spectroelectrochemical and transient absorption measurements of betanin adsorbed on TiO_2 are reported and interpreted with the help of time-dependent DFT calculations. Overlapping optical transitions of the excited state of Bt and the ground state of various intermediates complicate the interpretation of the data, but taken together, experiment and theory support the conclusion that excited state betanin is capable of simultaneous two-electron injection into the conduction band of TiO_2. Nanosecond transient absorption data are tentatively ascribed to the appearance of a radical quinonoid species resulting from recombination of injected electrons to form the one-electron oxidation product of Bt. We suggest that this recombination limits the maximum photovoltage of betanin-based dye-sensitized solar cells and their long-term stability. The present results are guiding ongoing efforts to improve the performance of Bt-based DSSCs through variations in the redox mediator and by tuning the molecular properties of the dye to enhance stability. The work presented here suggests that proton-coupled redox mediators would be more effective than the frequently used iodide/triiodide redox couple. In future work, we will also explore the performance of copigmented betalains known for enhanced stability.

■ ASSOCIATED CONTENT

Supporting Information

The Supporting Information is available free of charge on the ACS Publications website at DOI: 10.1021/acs.jpcc.5b05896.

> Absorption spectra of betanin on TiO_2 and ZrO_2 as a function of dye loading (Figure S1), global fits to transient spectra of betanin on TiO_2 and ZrO_2 (Figure S2), optical absorption spectra of betanin in aqueous solution before and after enzymatic oxidation (Figure S3), exponential fits to nanosecond transients (Figure S4), and trends in computed absorption wavelengths for different functionals and polarizable continuum models (Table S1) (PDF)

■ AUTHOR INFORMATION

Corresponding Author

*(J.L.M.) E-mail: jmchale@wsu.edu.

Notes

The authors declare no competing financial interest.

■ ACKNOWLEDGMENTS

The support of National Science Foundation Grant DMR-1305592 is gratefully acknowledged. A.M. and J.-E.M. acknowl-

edge the Swiss National Science Foundation and NCCR-MUST.

REFERENCES

(1) O'Regan, B.; Grätzel, M. A low-cost, high-efficiency solar cell based on dye-sensitized colloidal titanium dioxide films. *Nature* **1991**, *353*, 737−740.
(2) Yum, J.-H.; Baranoff, E.; Wenger, S.; Nazeeruddin, Md. K.; Grätzel, M. Panchromatic engineering for dye-sensitized solar cells. *Energy Environ. Sci.* **2011**, *4*, 842−957.
(3) Wang, Z.-S.; Koumura, N.; Cui, Y.; Miyashita, M.; Mori, S.; Hara, K. Exploitation of ionic liquid electrolyte for dye-sensitized solar cells by molecular modification of organic dye-sensitizers. *Chem. Mater.* **2009**, *21*, 2810−2816.
(4) Nazeeruddin, M. K.; Zakeeruddin, S. M.; Humphrey-Baker, R.; Jirousek, M.; Liska, P.; Vlachopoulos, N.; Shklover, V.; Fischer, C.-H.; Grätzel, M. Acid-base equilibria of (2,2′-bipyridyl-4,4′-dicarboxylic acid)ruthenium complexes and the effect of protonation on charge-transfer sensitization of nanocrystalline titania. *Inorg. Chem.* **1999**, *38*, 6298−6305.
(5) Calogero, G.; Bartolotta, A.; Di Marco, D.; Di Carlo, A.; Bonaccorso, F. Vegetable-based dye-sensitized solar cells. *Chem. Soc. Rev.* **2015**, *44*, 3244−3294.
(6) Zhang, D.; Lanier, S.; Downing, J. A.; Avent, J.; McHale, J. L. Betalain pigments for dye-sensitized solar cells. *J. Photochem. Photobiol., A* **2008**, *195*, 72−80.
(7) Sandquist, C.; McHale, J. L. Improved efficiency of betanin-based dye-sensitized solar cells. *J. Photochem. Photobiol., A* **2011**, *221*, 90−97.
(8) McHale, J. L. Light-harvesting chromophore aggregates and their potential for solar energy conversion. *J. Phys. Chem. Lett.* **2012**, *3*, 587−597.
(9) Calogero, G.; Yum, J.-H.; Sinopoli, A.; Di Marco, G.; Grätzel, M.; Nazeeruddin, M. K. Anthocyanins and betalains as light-harvesting pigments for dye-sensitized solar cells. *Sol. Energy* **2012**, *86*, 1563−1575.
(10) Calogero, G.; di Marco, G.; Caramori, S.; Cazzanti, S.; Argazzi, R.; Bignozzi, C. A. Natural dye-sensitizers for photoelectrochemical cells. *Energy Environ. Sci.* **2009**, *2*, 1162−1172.
(11) Hernandez-Martinez, A. R.; Estevez, M.; Vargas, S.; Rodriguez, R. Stabilized conversion efficiency and dye-sensitized solar cells from Beta vulgaris pigment. *Int. J. Mol. Sci.* **2013**, *14*, 4081−4093.
(12) Strack, D.; Vogt, T.; Schliemann, W. Recent advances in betalain research. *Phytochemistry* **2003**, *62*, 247−269.
(13) Martínez-Parra, J.; Muñoz, R. An Approach to characterization of betanine oxidation catalyzed by horseradish peroxidase. *J. Agric. Food Chem.* **1997**, *45*, 2984−2988.
(14) Martínez-Parra, J.; Muñoz, R. Characterization of betacyanin oxidation catalyzed by a peroxidase from *Beta vulgaris* L. roots. *J. Agric. Food Chem.* **2001**, *49*, 4064−4068.
(15) Butera, D.; Tesoriere, L.; Di Gaudio, F.; Bongiorno, A.; Allegra, M.; Pintaudi, A. M.; Kohen, R.; Livrea, M. A. Antioxidant activities of sicilian prickly pear (*Opuntia ficus indica*) fruit extracts and reducing properties of its betalains: betanin and indicaxanthin. *J. Agric. Food Chem.* **2002**, *50*, 6895−6901.
(16) Tesoriere, L.; Butera, D.; Allegra, M.; Fazzari, M.; Livrea, M. A. Distribution of betalain pigments in red blood cells after consumption of cactus pear fruits and increased resistance of the cells to ex vivo induced oxidative hemolysis in humans. *J. Agric. Food Chem.* **2005**, *53*, 1266−1270.
(17) Stintzing, F. C.; Herbach, K. M.; Mosshamer, M. R.; Carle, R.; Yi, W.; Sellappan, S.; Akoh, C. C.; Bunch, R.; Felker, P. Color, betalain pattern, and antioxidant properties of cactus pear (*Oppuntia* spp.) clones. *J. Agric. Food Chem.* **2005**, *53*, 442−451.
(18) Wybraniec, S.; Stalica, P.; Spórna, A.; Nemzer, B.; Pietrzkowski, Z.; Michałowski, T. Antioxidant activity of betanidin: electrochemical study in aqueous media. *J. Agric. Food Chem.* **2011**, *59*, 12163−12170.
(19) Wybraniec, S.; Michałowski, T. New pathways of betanidin and betanin enzymatic oxidation. *J. Agric. Food Chem.* **2011**, *59*, 9612−9622.
(20) Wybraniec, S.; Starzak, K.; Skopińska, A.; Nemzer, B.; Pietrzkowski, Z.; Michałowski, T. Studies on nonenzymatic oxidation mechanisms in neobetanin, betanin, and decarboxylated betanins. *J. Agric. Food Chem.* **2013**, *61*, 6465−6476.
(21) Cal, Y.; Sun, M.; Corke, H. Antioxidant activity of betalains from plants of the amaranthaceae. *J. Agric. Food Chem.* **2003**, *51*, 2288−2294.
(22) Gandía-Herrero, F.; Escribano, J.; García-Carmona, F. Characterization of the monophenolase activity of tyrosinase on betaxanthins: the tyramine-betaxanthin/dopamine-betaxanthin pair. *Planta* **2005**, *222*, 307−318.
(23) Herbach, K. M.; Stintzing, F. C.; Carle, R. Impact of thermal treatment on color and pigment pattern of red beet (*Beta vulgaris* L.) preparations. *J. Food Sci.* **2004**, *69*, C491−C498.
(24) Simon, J. D.; Peles, D. N. The red and the black. *Acc. Chem. Res.* **2010**, *43*, 1452−1460.
(25) Gauden, M.; Pezella, A.; Panzella, L.; Neves-Peterson, M. T.; Skovsen, E.; Peterson, S. B.; Mullen, K. M.; Napolitano, A.; d'Ischia, M.; Sundström, V. Role of solvent, pH, and molecular size in excited state deactivation of key eumelanin building blocks: implications for melanin pigment photostability. *J. Am. Chem. Soc.* **2008**, *130*, 17038−17043.
(26) Stark, K. B.; Gallas, J. M.; Zajac, G. W.; Golab, J. T.; Gidanian, S.; McIntire, T.; Farmer, P. J. Effects of stacking and redox state on optical absorption of melanins. Comparison of theoretical and experimental results. *J. Phys. Chem. B* **2005**, *109*, 1970−1977.
(27) Knorr, F. J.; Malamen, D. J.; McHale, J. L.; Marchioro, A.; Moser, J.-E. Two-electron photo-oxidation of betanin on titanium dioxide and potential for improved dye-sensitized solar energy conversion. *Proceedings, SPIE 9165, Physical Chemistry of Interfaces and Nanomaterials XIII* **2014**, 91650N.
(28) Frisch, M. J.; Trucks, G. W.; Schlegel, H. B.; Scuseria, G. E.; Robb, M. A.; Cheeseman, J. R.; Scalmani, G.; Barone, V.; Mennucci, B.; Petersson, G. A. et al. *Gaussian 09*, revision D.01; Gaussian, Inc.: Wallingford, CT, USA, 2009.
(29) Becke, A. D. Density-functional thermochemistry. III. The role of exact exchange. *J. Chem. Phys.* **1993**, *98*, 5648−5652.
(30) Lee, C.; Yang, W.; Parr, R. G. Development of Colle-Salvetti correlation-energy formula into a functional of the electron density. *Phys. Rev. B: Condens. Matter Mater. Phys.* **1988**, *37*, 785−789.
(31) Dunning, T. H., Jr. Gaussian basis sets for use in correlated molecular calculations. I. The atoms boron through neon and hydrogen. *J. Chem. Phys.* **1989**, *90*, 1007−1023.
(32) Woon, D. E.; Dunning, T. H., Jr. Gaussian basis sets for use in correlated molecular calculations. V. Core-valence basis sets for basis sets for boron through neon. *J. Chem. Phys.* **1995**, *103*, 4572−4585.
(33) Yanai, T.; Tew, D. P.; Handy, N. C. A new hybrid exchange-correlation functional using the Coulomb-attenuating method (CAM-B3LYP). *Chem. Phys. Lett.* **2004**, *393*, 51−57.
(34) Tawada, Y.; Tsuneda, T.; Yagaisawa, S.; Yanai, T.; Hirao, K. A long-range corrected time-dependent density functional theory. *J. Chem. Phys.* **2004**, *120*, 8425−8433.
(35) Vydrov, O. A.; Scuseria, G. E. Assessment of long-range corrected hybrid functional. *J. Chem. Phys.* **2006**, *125*, 234109/1.
(36) Vydrov, O. A.; Heyd, J.; Krukau, A.; Scuseria, G. E. Importance of short-range versus long-range Hartree-Fock exchange for the performance of hybrid density functional. *J. Chem. Phys.* **2006**, *125*, 074106/1.
(37) Vyrdrov, O. A.; Scuseria, G. E.; Perdew, J. P. Tests of functional for systems with fractional electron number. *J. Chem. Phys.* **2007**, *126*, 154109/1.
(38) Jacquemin, D.; Perpete, E. A.; Ciofini, I.; Adamo, C. Assessment of the ωB97 family of excited state calculations. *Theor. Chem. Acc.* **2011**, *128*, 127−136.
(39) Schreiber, M.; Silva-Junior, M. R.; Sauer, S. P. A.; Thiel, W. Benchmarks for electronically excited states, CASPT2, CC2, CCSD, and CC3. *J. Chem. Phys.* **2008**, *128*, 134110/1.

DOI: 10.1021/acs.jpcc.5b05896
J. Phys. Chem. C 2015, 119, 19030−19041

(40) Silva-Junior, M. R.; Sauer, S. P. A.; Schreiber, M.; Thiel, W. Basis set effects on coupled cluster benchmarks of electronically excited states: CC3, CCSDR(3), and CC2. *Mol. Phys.* **2010**, *108*, 453−465.
(41) Jacquemin, D.; Mennucci, B.; Adamo, C. Excited state calculations with TD-DFT: from benchmarks to simulations in complex environments. *Phys. Chem. Chem. Phys.* **2011**, *13*, 16987−16998.
(42) Leang, S. S.; Zahariev, F.; Gordon, M. S. Benchmarking the performance of time-dependent density functional methods. *J. Chem. Phys.* **2012**, *136*, 104101/1.
(43) Laurent, A. D.; Jacquemin, D. TD-DFT benchmarks, a review. *Int. J. Quantum Chem.* **2013**, *113*, 2019−2039.
(44) Peach, M. J. G.; Benfield, P.; Helgaker, T.; Tozer, D. J. Excitation energies in density functional theory: an evaluation and a diagnostic test. *J. Chem. Phys.* **2008**, *128*, 044118/1.
(45) Rohrdanz, M. A.; Martins, K. M.; Herbert, J. M. A long-range density functional that performs well for both ground-state properties and TD-DFT excitation energies, including charge-transfer excited states. *J. Chem. Phys.* **2009**, *130*, 054112/1.
(46) Alipour, M. How does LCDFT compare to SAC-CI for the treatment of valence and Rydberg excited states of organic compounds? *J. Phys. Chem. A* **2014**, *118*, 1741−1747.
(47) Marenich, A. V.; Cramer, C. J.; Truhlar, D. G. Universal solvation model based on solute electron density and on a continuum model of the solvent defined by the bulk dielectric constant and the atomic surface tension. *J. Phys. Chem. B* **2009**, *113*, 6378−6396.
(48) Redmond, G.; Fitzmaurice, D. Spectroscopic determination of flatband potentials for polycrystalline TiO_2 electrode in nonaqueous solvents. *J. Phys. Chem.* **1993**, *97*, 1426−1430.
(49) Schwartz, S. J.; Von Elbe, J. H. Quantitative determination of individual betacyanin pigments by high-performance liquid chromatography. *J. Agric. Food Chem.* **1980**, *28*, 540−543.
(50) Brede, O.; Kapoor, S.; Mukherjee, T.; Hermann, R.; Naumov, S. Diphenol radical cations and semiquinone radicals as direct products of electron transfer from catechol, resorcinol, and hydroquinone to parent solvent radical cations. *Phys. Chem. Chem. Phys.* **2002**, *4*, 5096−5104.
(51) Grilj, J.; Todorova, T. K.; Yi, C.; Liu, S.-X.; Vauthey, E.; Decurtins, S. A spectroscopic and computational study of a photoinduced cross-dehydrogenation coupling reaction of a stable semiquinone radical. *Chem.−Eur. J.* **2012**, *18*, 13605−13608.
(52) Edge, R.; d'Ischia, M.; Land, E. J.; Napolitano, A.; Navaratnam, S.; Panzella, L.; Pezella, A.; Ramsden, C. A.; Riley, P. A. Dopaquinone redox exchange with dihydroxyindole and dihydroxyindole carboxylic acid. *Pigm. Cell Res.* **2006**, *19*, 443−450.
(53) Evans, D. H. One-electron and two-electron transfers in electrochemistry and homogeneous solution ractions. *Chem. Rev.* **2008**, *108*, 2113−2144.
(54) Lopez-Tenez, M.; Gonzalez, J.; Molina, A. Two-electron transfer reactions in electrochemistry for solution-soluble and surface-confined molecules: a common approach. *J. Phys. Chem. C* **2014**, *118*, 12312−12324.
(55) Sugumaran, M.; Semensi, V. Quinone methide as a new intermediate in eumelanin biosynthesis. *J. Biol. Chem.* **1991**, *266*, 6073−6068.
(56) Rex, R. E.; Knorr, F. J.; McHale, J. L. Surface traps of TiO_2 nanosheets and nanoparticles as illuminated by spectroelectrochemical photoluminescence. *J. Phys. Chem. C* **2014**, *118*, 16831−16841.
(57) Ohno, T.; Izumi, S.; Fujihara, K.; Masaki, Y.; Matsumara, M. Vanishing of current-doubling effect in photooxidation of 2-propanol on TiO_2 in solutions containing Fe(III) ions. *J. Phys. Chem. B* **2000**, *104*, 6801−6803.
(58) Zweigle, G. C.; McHale, J. L. Theory of transition-dipole coupling in dye-sensitized semiconductor nanoparticles. *J. Phys. Chem. C* **2011**, *115*, 13693−13703.
(59) Ito, S. A chemist's view of melanogenesis. *Pigm. Cell Res.* **2003**, *16*, 230−236.
(60) Stark, K. B.; Gallas, J. M.; Zajac, G. W.; Golab, J. T.; Gidanian, S.; McIntire, T.; Farmer, P. J. Effect of stacking and redox site on optical absorption spectra of melanins − Computational and experimental results. *J. Phys. Chem. B* **2005**, *109*, 1970−1977.
(61) Sampaio, R. N.; O'Donnell, R. M.; Barr, T. J.; Meyer, G. J. Electric fields control $TiO_2(e^-)$ and $I_3^- \rightarrow$ charge recombination in dye-sensitized solar cells. *J. Phys. Chem. Lett.* **2014**, *5*, 3265−3268.
(62) Rowley, J. G.; Farnum, B. H.; Ardo, S.; Meyer, G. J. Iodide chemistry in dye-sensitized solar cells: making and breaking I-I bonds for solar energy conversion. *J. Phys. Chem. Lett.* **2010**, *1*, 3132−3140.
(63) O'Regan, B. C.; Durrant, J. R. Kinetic and energetic paradigms for dye-sensitized solar cells: moving from the ideal to the real. *Acc. Chem. Res.* **2009**, *42*, 1799−1808.

DOI: 10.1021/acs.jpcc.5b05896
J. Phys. Chem. C 2015, 119, 19030−19041

Dynamics of Interfacial Electron Transfer from Betanin to Nanocrystalline TiO_2: The Pursuit of Two-Electron Injection

Fritz J. Knorr,[a] Jeanne L. McHale,[*a] Aurora E. Clark,[a]
Arianna Marchioro,[b] and Jacques-E. Moser[b]

[a]Department of Chemistry, Washington State University Box 644630
Pullman, WA 99164-4630 USA

[b]Photochemical Dynamics Group, Institute of Chemical Sciences and Engineering
École Polytechnique Fédérale de Lausanne
CH-1015 Lausanne, Switzerland

Supporting Information

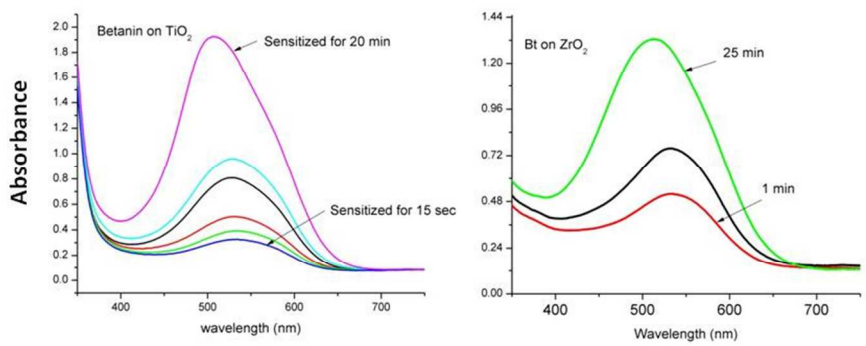

Fig. S1. Absorption spectra of betanin on TiO_2 (left) and ZrO_2 (right) as a function of sensitization time, showing blue shift as dye loading increases.

[*] Corresponding author, jmchale@wsu.edu

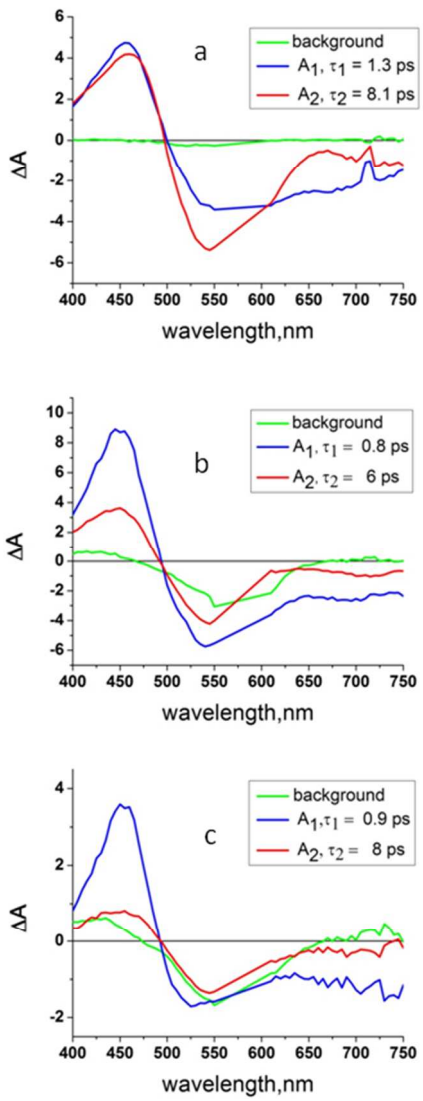

Fig. S2 Global fits to transient spectra of a) Bt on ZrO_2 in contact with MPN, b) Bt on TiO_2 in contact with MPN, and c) Bt on TiO_2 in contact with a solution of LiI in MPN. Captions show the decay times from a fit to a bi-exponential plus nondecaying background.

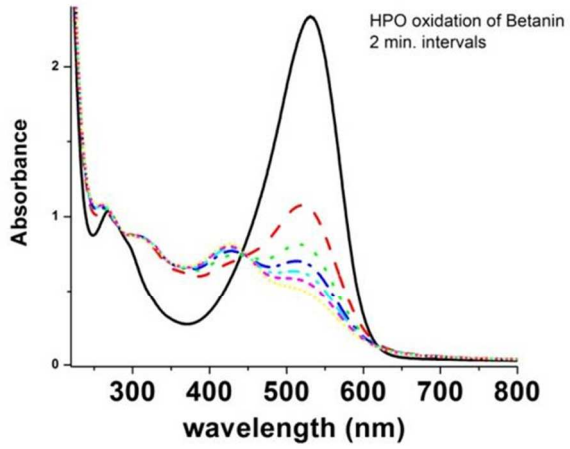

Fig. S3 Absorption spectrum of Bt before (black trace) and at 2-minute intervals (dashed curves) after adding horseradish peroxidase, showing formation of a product with an absorption band near 430 nm.

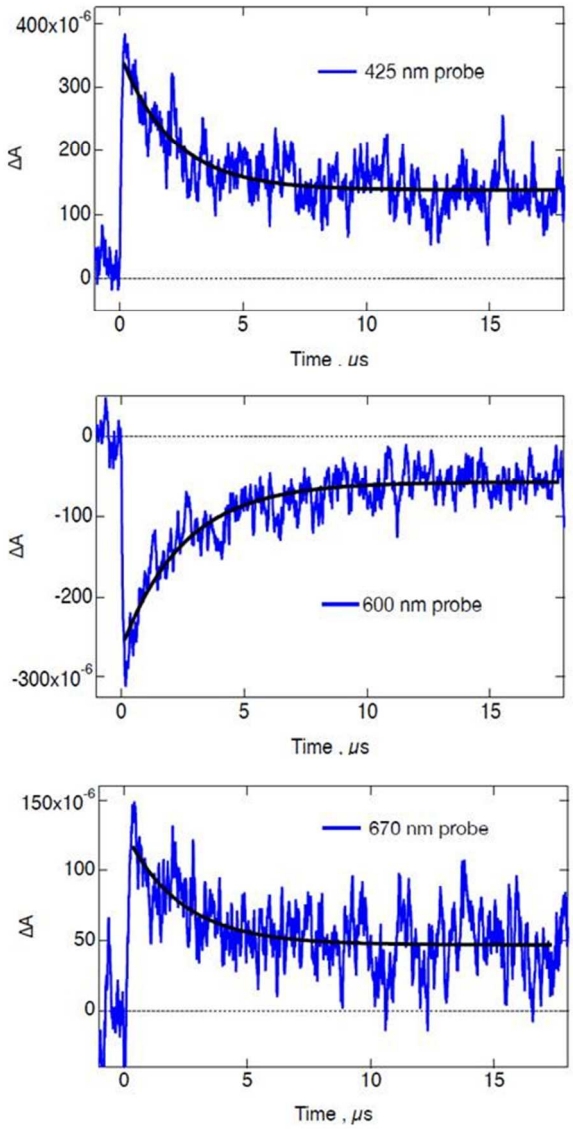

Fig. S4. Nanosecond transients for Bt on TiO_2 in the presence of MPN at 425 nm (top), 600 nm (middle) and 670 nm (bottom), with a pump wavelength of 530 nm. The black traces are the fits to a single exponential plus a non-decaying component.

Table S1. Computed excitation wavelengths (in nm) of molecules **I** and **VI** at the B3LYP/cc-pVDZ optimized geometry. The $S_0 \rightarrow S_x$ transition is examined where *x* is the state that has the largest predicted oscillator strength, with TD-DFT calculations employing the B3LYP, cam-B3LYP, and lc-ωPBE density functionals in the gas-phase and using different polarizable continuum models to approximate the affect of bulk aqueous solution. The excitation energy is compared to the experimental λ_{max}.

	I	**VI**	$\Delta\ \lambda_{max}$ (**I – VI**)
Expt (nm)	530	445	85
B3LYP gas	514	522	-8
B3LYP CPCM	504	488	16
B3LYP IEF-PCM	501	485	16
B3LYP SMD	496	480	16
lc-ωPBE gas	442	408	34
lc-ωPBE CPCM	425	442	-17
lc-ωPBE IEF-PCM	424	439	-15
lc-ωPBE SMD	420	441	-21
cam-B3LYP gas	478	439	39
cam-B3LYP CPCM	456	433	23
cam-B3LYP IEF-PCM	454	432	22
cam-B3LYP SMD	447	463	-16